DIFFRACTION TRAVELTIMES AS MOVEOUT FUNCTION FOR VELOCITY ANALYSIS

T. Klüver

email: *tilman.kluever@gpi.uni-karlsruhe.de*

keywords: *tomography, migration, velocity model building*

ABSTRACT

In this paper, a new inversion scheme for the determination of migration depth velocity models is presented. The method explicitly enforces the kinematic equivalence between common image gathers and common reflection point gathers. The use of diffraction traveltime operators as moveout functions allows to extract differences in time dip with respect to the illumination angle along the CRP trajectory. The minimization of these time dip residuals in combination with traveltime residuals leads to a consistent geological dip for all offsets or scattering angles which might not be obtained by flattening either common image gathers or common reflection point gathers only. The inversion scheme will be presented in detail and the results of a first application to a synthetic data example will be shown.

INTRODUCTION

A common way to determine a suitable velocity model for depth migration is based on the analysis of the flatness of common image gathers (CIG). This is done either for selected analysis locations or horizon based in a layer stripping fashion. Knowing the geological dip, the picked depth residuals may be converted to traveltime misfits which may be used for a tomographic update of the velocity model (see, e. g., Stork, 1992). The basic assumption behind this approach is that a CIG contains all information stemming from the same depth point. However, this only holds when the true velocity model is known. Generally, a CIG deviates kinematically from a common reflection point (CRP) gather, which contains all information stemming from a selected depth point in a specified velocity model. The CRP gather may be obtained by selecting all traces from the prestack data with source and receiver locations determined by ray tracing in the current depth model, consisting of the velocity itself, the depth position of interest, and the geological dip at that position. Thus, the CRP gather is model dependent. If the depth model is consistent with the prestack data for that position, the CRP gather and the CIG must be kinematically identical. This condition ensures that all traces in the CRP gather are traces containing a stationary point, i. e. a point of tangency between the diffraction traveltime operator and the actual diffraction/reflection event in the prestack data. The kinematic equivalence between CRP gather and CIG not only implies a flat CIG but also the same geological dip in all depth migrated common offset or common scattering angle sections. Only then an accurate focusing of the migrated energy can be obtained.

In this paper, I present a method to enforce the kinematic equivalence between CRP gather and CIG in a tomographic inversion scheme for the 2D case. The method uses sparse analysis locations selected in the zero offset (ZO) poststack time domain. Each pick location is assumed to be on an unconverted primary event. These pick locations, described by their trace location, the two-way ZO traveltime and the ZO time dip are transformed into depth positions by normal ray depth migration in an initial velocity model. In this way, an initial estimate of the geological dip at these depth points is obtained. Then traveltime residuals and dip difference between diffraction traveltime operator and the event in the prestack data are extracted using the diffraction traveltime operator as a moveout function. This procedure is described in detail later on. The time and time dip residuals are used for a tomographic update of the depth model.

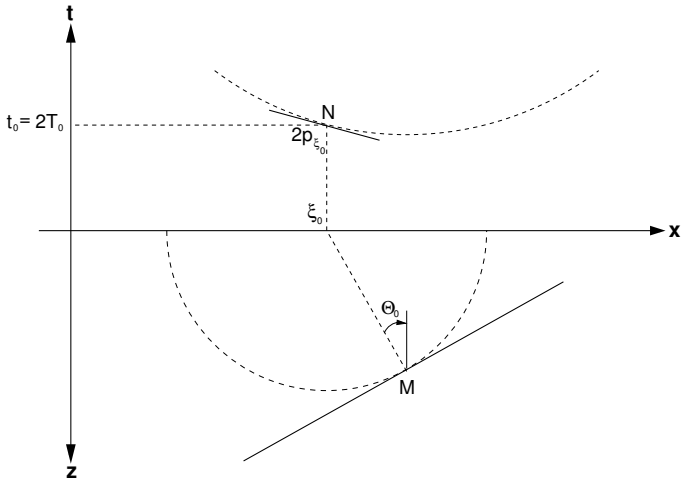

Figure 1: Relationship between time and depth domain for the ZO case. See main text for details.

DIFFRACTION TRAVELTIMES AS MOVEOUT FUNCTION

The core of the presented method is the use of diffraction traveltime operators as moveout functions. The diffraction traveltime operator for a specific depth point is used in Kirchhoff depth migration as surface along which all energy is summed up to be assigned to the corresponding depth position. If there exists a point of tangency between the diffraction traveltime operator and an event in the prestack data, this summation is constructive. The point of tangency is called stationary point. Any selected, at least locally coherent event in the ZO poststack time domain describes an estimate of the ZO stationary point, characterized by the ZO two-way traveltime, the trace position, and the time dip in the ZO section. The corresponding depth position and geological dip may be found by normal ray depth map migration. Performing ray tracing in the opposite direction the ZO stationary point is forward-modeled again. Note that this holds in principal for any velocity model. This means that for ZO the kinematic equivalence between CRP gather and CIG may be assured any time. In Figure 1 the relationship between time and depth domain is depicted for the ZO case. The locally coherent event N in the time domain (solid line in the upper half-space) is described by its lateral position ξ_0, the ZO two-way time $t_0 = 2\,T_0$ and the time dip $2\,p_{\xi_0}$, where p_{ξ_0} denotes the horizontal component of the slowness vector and T_0 is the ZO one-way traveltime. Associated with event N is point M located on a reflector in the depth domain where the ZO ray (indicated by the dashed line connecting ξ_0 and M) hits the reflector normally. The dashed half-circle in the depth domain indicates the ZO isochron, i. e. the line of equal two-way traveltime t_0 which is tangent to the reflector at point M. The counterpart to the isochron is the ZO diffraction traveltime curve depicted as dashed curved line in the time domain. The diffraction traveltime curve is tangent to the locally coherent event at the stationary point N. The local geological dip at point M is given by Θ_0. It is measured from the normal ray to the vertical with the vertical pointing upwards and, thus, against the depth axis. This definition is used in this paper for all rays starting at point M. The angle between an arbitrary ray and the vertical will be denoted by γ. Angles are defined to be positive if they are measured counterclockwise and vice versa. This definition ensures that the sign of the initial horizontal slowness component of a ray starting at point M equals the sign of the angle between the ray and the vertical, i. e. $p_x(M) = \sin(\gamma)/v(M)$, where $v(M)$ is the wave propagation velocity at point M.

Once the depth position corresponding to a selected pick in the ZO section has been found the diffraction traveltime operator for that position can be forward-modeled using ray tracing. Alternatively, it may be extracted from a Greens function table (GFT) for Kirchhoff migration. The diffraction traveltime function τ_M for point M is given by traveltimes along all ray pairs connecting a source S with a receiver G, both at the surface, through point M. This means that the diffraction traveltimes are a function of source and receiver coordinates, i. e. $\tau_M = \tau_M(x_S, x_G)$. These, in turn, are functions of the corresponding take-off

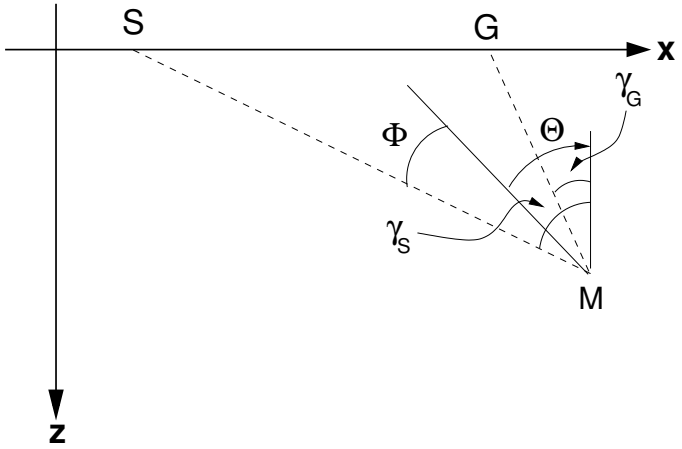

Figure 2: Definition of illumination and scattering angle. See main text for details.

angles γ_S and γ_G. Defining the scattering angle Φ and the illumination angle Θ to be

$$\Phi = (\gamma_S - \gamma_G)/2 \,, \qquad \Theta = (\gamma_S + \gamma_G)/2 \,, \tag{1}$$

the diffraction traveltime operator becomes a function of these angles: $\tau_M = \tau_M(\Theta, \Phi)$. For a graphical explanation of Θ and Φ see Figure 2. Note the analogy between the angle domain and the commonly used midpoint-offset domain: shot and receiver coordinates at the surface correspond to take-off angles in depth, the midpoint coordinate $\xi = (x_S + x_G)/2$ corresponds to illumination angle Θ, and the half-offset $h = (x_S - x_G)/2$ corresponds to scattering angle Φ. This, in general, non-linear relation is described in detail below.

For using τ_M as moveout function the diffraction traveltime operator is defined as surface of traveltime zero. In that way, every trace within the migration aperture is associated with a different delay time and traveltime is measured with respect to the diffraction traveltime. This means that directly traveltime residuals are measured. This transformation is unique for a selected depth position and velocity model. It changes for different depth positions and different velocity models.

As an example, I demonstrate this transformation using a simple model: point M is located at $x = 0\,\mathrm{m}$ and $z = 3500\,\mathrm{m}$ on a reflector with a dip of 15° and a homogeneous overburden with a wave propagation velocity of $2000\,\mathrm{m/s}$. Traveltime as a function of midpoint and offset of the corresponding reflection event in the prestack data is shown in Figure 3(a). In Figure 3(b) the same traveltimes are shown as a function of scattering and illumination angle. Whereas the traveltimes correspond to specular reflections occurring anywhere on the reflector the angles correspond to mostly non-specular rays which all start at point M. These are the angles of the ray pairs building the diffraction traveltime operator of point M which is shown in Figure 3(c) in the midpoint-offset domain and in Figure 3(d) in the angle domain. Figure 3(e) and 3(f) show the difference between reflection and diffraction traveltimes in the midpoint-offset and angle domain, respectively. In all Figures, the CRP trajectory is highlighted as dashed-dotted line. The CRP trajectory is given as that line along which the traveltime difference vanishes. Generally, it is a curved line in the midpoint-offset domain. In the angle domain it simplifies to a straight line because the illumination angle must equal the geological dip. This can clearly be seen in Figure 3(f). Figure 4 shows time dips, i.e. the first partial derivative of traveltime with respect to midpoint and illumination angle, respectively. Sub-figures are ordered the same way as in Figure 3. As the CRP trajectory is built of specular reflections, not only the traveltime difference but also the time dip difference vanishes along it as can be seen in Figure 4(e) and Figure 4(f). Vanishing time and time dip difference between reflection and diffraction traveltime surface along the CRP trajectory is a necessary condition for correct subsurface imaging. This simply states that the CRP trajectory has to be a trajectory of stationary points. Note that the difference between time dip with respect to offset and scattering angle vanishes as soon as there is no difference between reflection and diffraction traveltimes.

Figures 5 and 6 show the same quantities for a wrong depth model. The velocity has been changed to

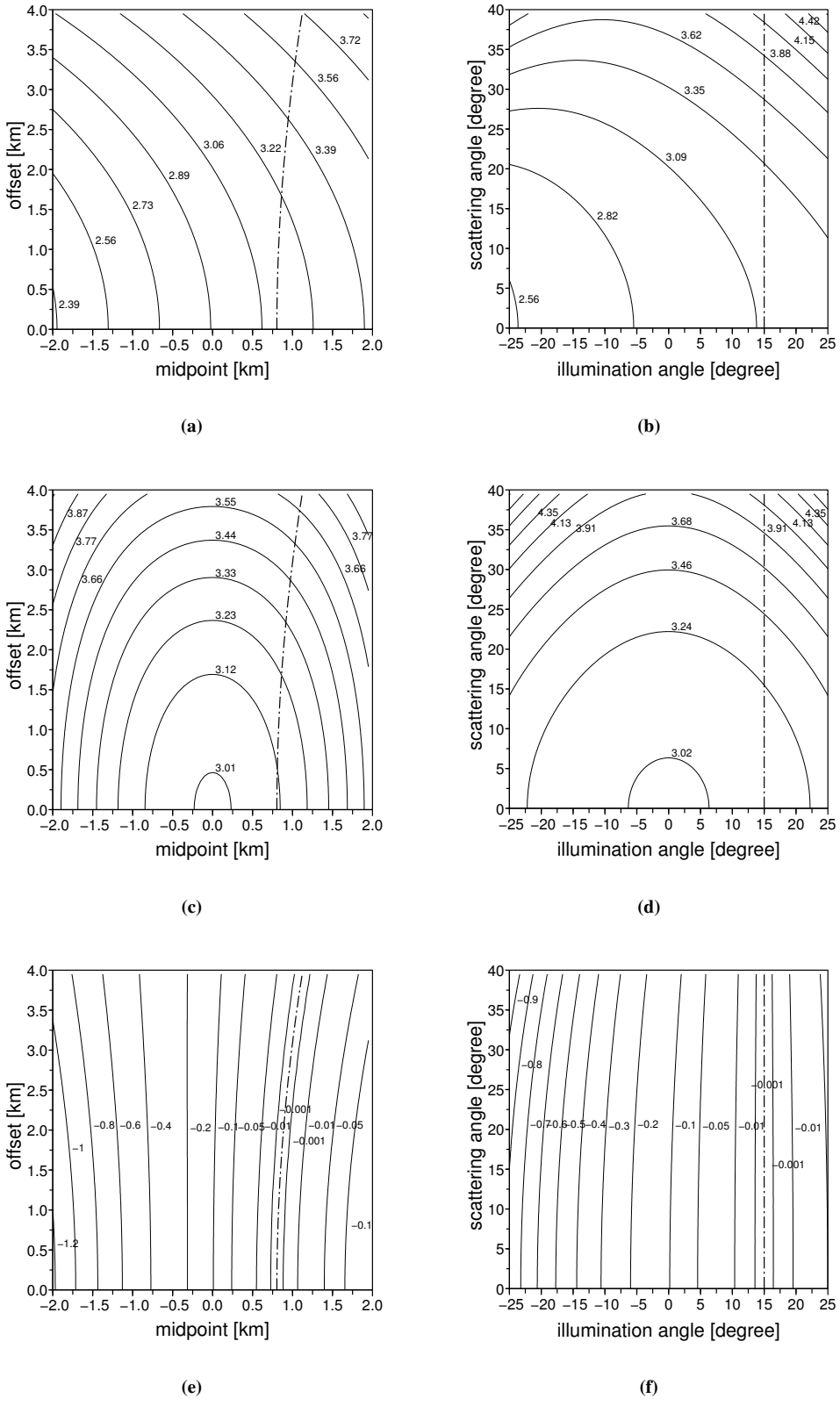

Figure 3: Correct velocity model: traveltime distribution [s] along the reflection event (a) in the midpoint-offset domain and (b) in the angle domain. Traveltime distribution along the diffraction traveltime operator (c) in the midpoint-offset domain and (d) in the angle domain. Traveltime difference between reflection event and diffraction traveltime operator (e) in the midpoint-offset domain and (f) in the angle domain.

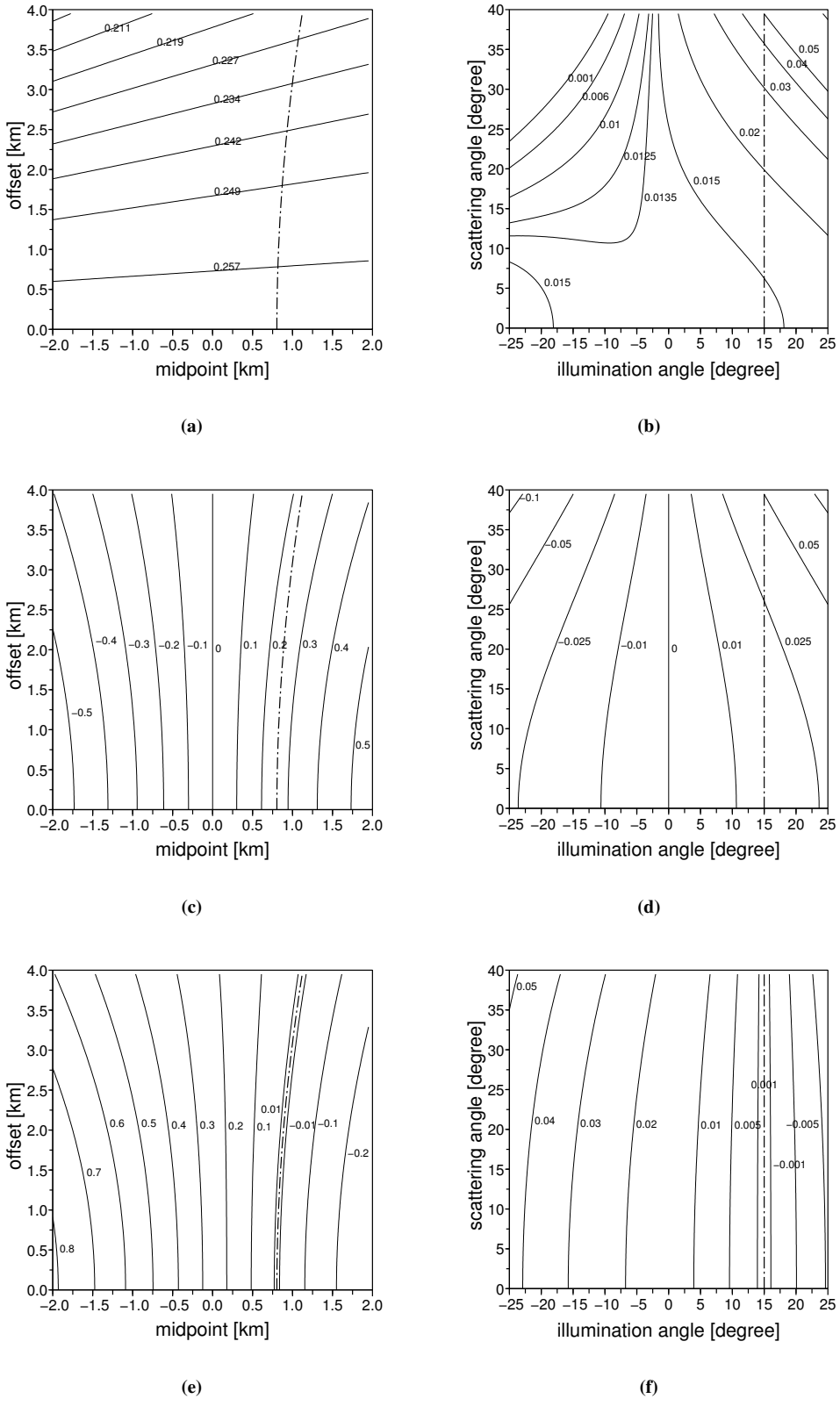

Figure 4: Correct velocity model: time dip distribution along the reflection event (a) in the midpoint-offset domain [s/km] and (b) in the angle domain [s/°]. Time dip distribution along the diffraction traveltime operator (c) in the midpoint-offset domain and (d) in the angle domain. Time dip difference between reflection event and diffraction traveltime operator (e) in the midpoint-offset domain and (f) in the angle domain.

2300 m/s. Point M has been chosen such that the ZO stationary point remains unchanged. Therefore, the CIG and CRP gather are kinematically equivalent for ZO. However, this no longer holds for finite offsets and finite scattering angles. In a wrong depth model the time and time dip difference no longer vanishes along the CRP trajectory. This is depicted in Figures 5(e) and 5(f) for the time difference and in Figures 6(e) and 6(f) for the time dip difference. The reflection traveltimes are fixed as they depend on the true velocity model. Diffraction traveltimes, angles, and the CRP trajectory are model dependent quantities. Thus, they have changed in the wrong model. This leads to the deviation of the CRP trajectory from a trajectory of stationary points.

THE IMAGING CONDITION

If point M corresponding to a ZO stationary point is positioned on a reflector the specular ray pairs are constrained to $\Theta = \Theta_0$, the traveltimes t along these ray pairs are given by the subset $t = \tau_M(\Theta = \Theta_0, \Phi)$ of the diffraction traveltime function. Source and receiver positions together with these traveltimes build up the CRP trajectory along which the energy stemming from point M can be found in the prestack data. However, for migrating this energy to point M it is not sufficient to find a velocity model, depth position and geological dip which explains the CRP trajectory only. It is also necessary that on each point on the CRP trajectory the diffraction traveltime function and the event in the prestack data have the same time dip with respect to the midpoint or illumination angle, respectively. Only then a constructive summation can be performed and all stationary points are aligned along the CRP trajectory. The goal of the inversion scheme presented below is to make the CRP trajectory and the CIG corresponding to each picked ZO stationary point kinematically equivalent.

THE INVERSION SCHEME

The determination of a subsurface velocity model states a nonlinear inverse problem. Here, I will use time and time dip residuals in an iterative tomographic inversion scheme for the determination of such a velocity model. The scheme tries to minimize a cost-function which is formulated in the least-squares sense.

Data and model components

The inversion starts with the selection of a number of picks in a ZO section which can be obtained by any stacking procedure. For each pick all quantities describing the ZO stationary point have to be determined. Corresponding initial estimates of the depth position and geological dip are determined in the initial velocity model using normal ray tracing. For the implementation I have chosen the same two dimensional B-spline representation (de Boor, 1978) of the velocity model as described in Duveneck (2002). This, together with a similar description of the ZO picks, makes the method presented in Duveneck (2002) and Duveneck (2004) ideal for the determination of an initial velocity model for the method presented here. The complete model description consists of all depth positions, geological dips and the B-spline coefficients representing the velocity distribution. All model components are summarized in the model vector $\mathbf{m}$:

$$\mathbf{m} = (x_i, z_i, \Theta_{0_i}, v_{jk})^T \ , \quad i = 1, \ldots, n_{\text{data}} \ , \quad j = 1, \ldots, n_x \ , \quad k = 1, \ldots, n_z \ , \tag{2}$$

where n_{data} is the number of picks in the ZO section. The number of B-spline nodes in horizontal and vertical direction is given by n_x and n_z, respectively.

For each depth point the diffraction traveltime operator is computed using ray tracing in the current velocity model. All traces within a user-given aperture are time shifted as described above. In this way, a small time-shifted prestack data cube in the angle domain is created for each pick. Inside these cubes time and time dip residuals for all scattering angles are extracted along the model based CRP trajectory. The necessary picking strategy is described below. Generally, this leads to a different number of picks in each cube which are summarized in a data misfit vector:

$$\Delta\mathbf{d}_{\text{Cube}_i} = \left(\Delta t_l, \left[\Delta\frac{\partial t}{\partial\Theta}\right]_l\right)^T_i \ , \quad i = 1, \ldots, n_{\text{data}} \ , \quad l = 1, \ldots, n_{\text{pick}} \ , \tag{3}$$

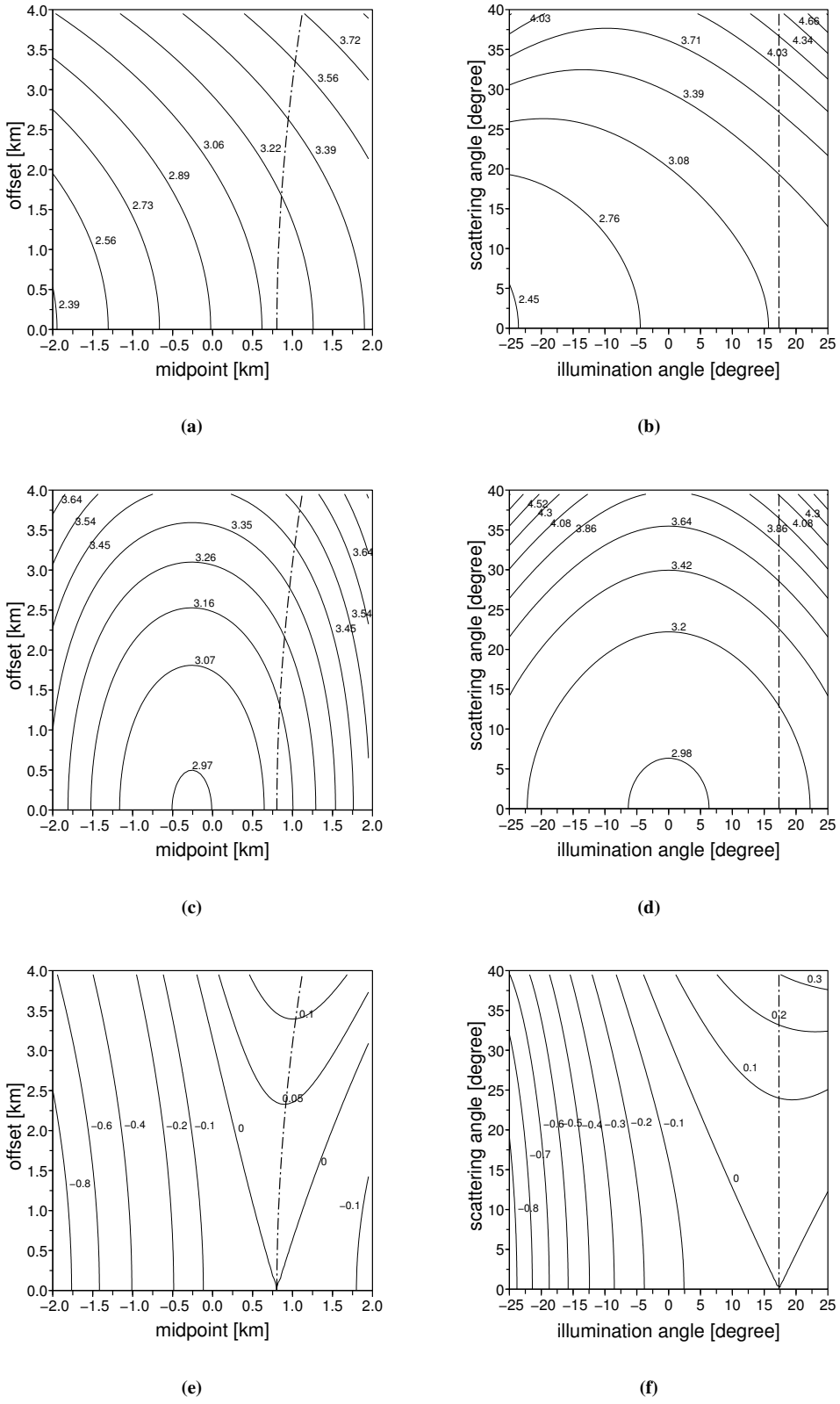

Figure 5: Wrong velocity model: traveltime distribution [s] along the reflection event (a) in the midpoint-offset domain and (b) in the angle domain. Traveltime distribution along the diffraction traveltime operator (c) in the midpoint-offset domain and (d) in the angle domain. Traveltime difference between reflection event and diffraction traveltime operator (e) in the midpoint-offset domain and (f) in the angle domain.

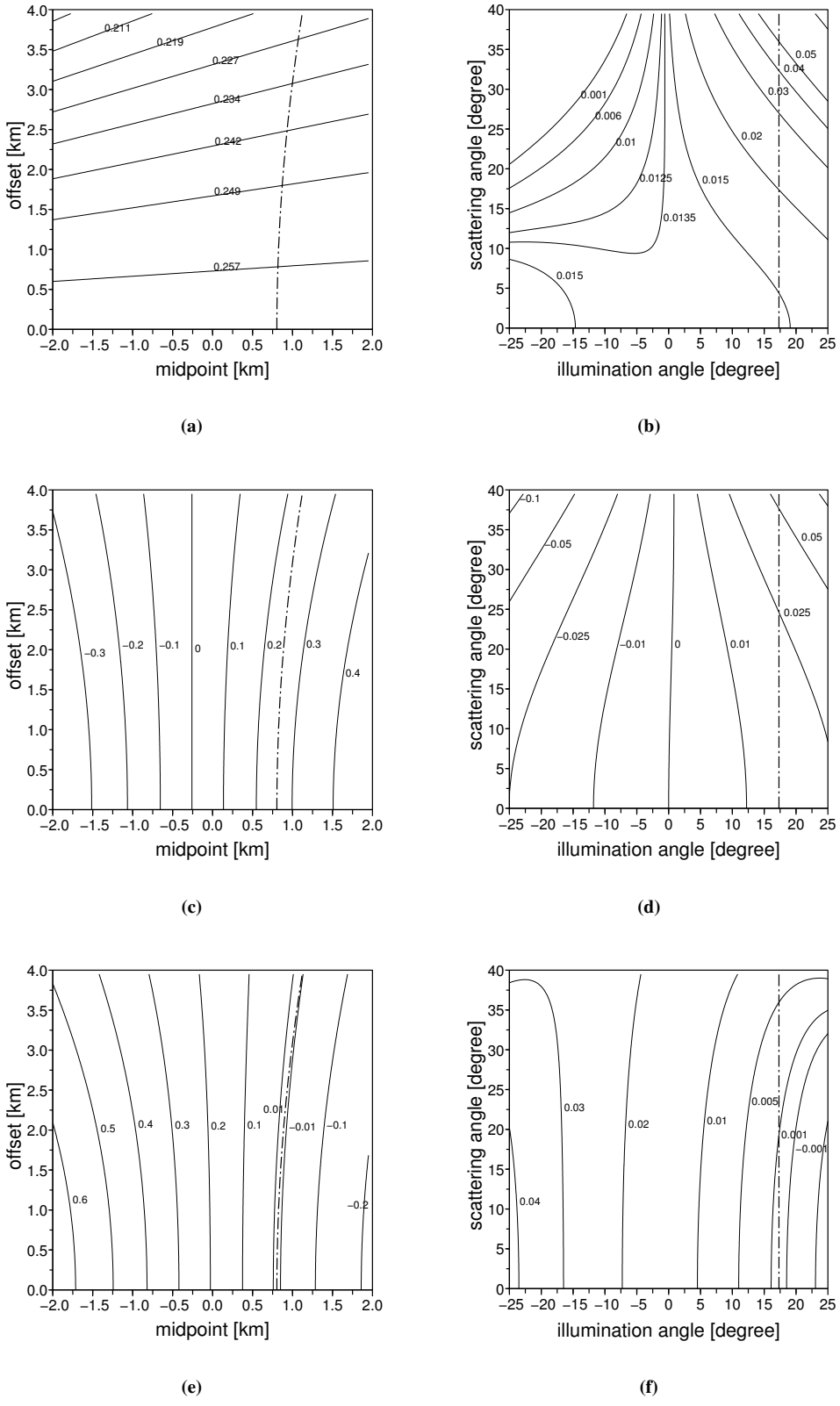

Figure 6: Wrong velocity model: time dip distribution along the reflection event (a) in the midpoint-offset domain [s/km] and (b) in the angle domain [s/°]. Time dip distribution along the diffraction traveltime operator (c) in the midpoint-offset domain and (d) in the angle domain. Time dip difference between reflection event and diffraction traveltime operator (e) in the midpoint-offset domain and (f) in the angle domain.

where n_{pick} denotes the number of picks in the i-th cube. These data misfits are used to update the depth model. This update is performed iteratively because of the nonlinearity of the corresponding inverse problem. Once a new model has been found the ZO picks may be used to obtain new estimates of the depth positions and geological dips by normal ray tracing. Alternatively, the estimates obtained by the inversion can be used. This means to allow errors in the ZO data components. Therefore, the ZO data misfit

$$\Delta\mathbf{d}_{ZO_i} = (\Delta T_0, \Delta p_{\xi_0}, \Delta\xi_0)_i^T \ , \quad i = 1, \ldots, n_{\text{data}} \ , \tag{4}$$

is part of the complete data misfit vector given by

$$\Delta\mathbf{d} = (\Delta\mathbf{d}_{ZO_i}, \Delta\mathbf{d}_{\text{Cube}_i})_i^T \ , \quad i = 1, \ldots, n_{\text{data}} \ . \tag{5}$$

Note that only the ZO data itself are known. All finite offset quantities are picked directly as data misfits. The true finite-offset data do not need to be known for the formulation of the inverse problem. The ZO data misfits are easily obtained by forward modeling using normal ray tracing.

The inverse problem and its solution

With the model and data misfit vectors defined above, the inverse problem may be formulated as follows:

Given a total number of n_{data} picks of stationary points in a ZO section, find a model described by model vector (2) in which the misfit between the picked ZO data components and the forward modeled ones as well as the picked time and time dip residuals in all time-shifted prestack data cubes is minimized. This problem is formulated as a least-squares problem (Menke, 1984; Tarantola, 1987). The optimum model is found by minimizing the cost-function

$$S(\mathbf{m}) = \frac{1}{2}\|\Delta\mathbf{d}(\mathbf{m})\|^2 = \frac{1}{2}\Delta\mathbf{d}^T(\mathbf{m})\underline{\mathbf{C}}_D^{-1}\Delta\mathbf{d}(\mathbf{m}) \ , \tag{6}$$

where $\underline{\mathbf{C}}_D$ denotes a symmetric, positive definite matrix weighting the different data components in the computation of S.

The data misfit vector $\Delta\mathbf{d}$ may be expressed as the difference between the true data vector $\mathbf{d}$ and the forward modeled data vector:

$$\Delta\mathbf{d} = \mathbf{d} - \mathbf{f}(\mathbf{m}) \tag{7}$$

where $\mathbf{f}(\mathbf{m})$ denotes the model dependent forward modeling operator. This operator is nonlinear due to the nonlinear dependence of ray tracing results on model parameters. For the iterative minimization of cost function S, it is assumed that the forward modeling operator may be linearized in the vicinity of the current model vector $\mathbf{m}_n$ of the n-th iteration:

$$\mathbf{f}(\mathbf{m}_n + \Delta\mathbf{m}) = \mathbf{f}(\mathbf{m}_n) + \underline{\mathbf{F}}\Delta\mathbf{m} \ . \tag{8}$$

Matrix $\underline{\mathbf{F}}$ contains the first partial derivatives of the data components with respect to the model components, also known as Fréchet derivatives.

A necessary condition for a minimum of S is

$$\nabla S = \mathbf{0} \ . \tag{9}$$

For a derivation of the resulting system of equations the reader is referred toDuveneck (2004). The solution of that system implies the computation of a matrix inverse. In order to compute this inverse in a stable way, the problem has to be regularized. This is done minimizing the second spatial derivatives of the velocity model in the same way as described in Duveneck (2004). In each iteration a model update vector $\Delta\mathbf{m}$ is computed. The updated model for the next iteration is given by

$$\mathbf{m}_{n+1} = \mathbf{m}_n + \lambda\Delta\mathbf{m} \ , \tag{10}$$

where the factor λ controls the length of the applied model update vector. The matrix to be inverted is sparse as each pick in the ZO section is independent of all others. To account for this sparseness the model update vector is computed using the LSQR algorithm (Paige and Saunders, 1982a,b).

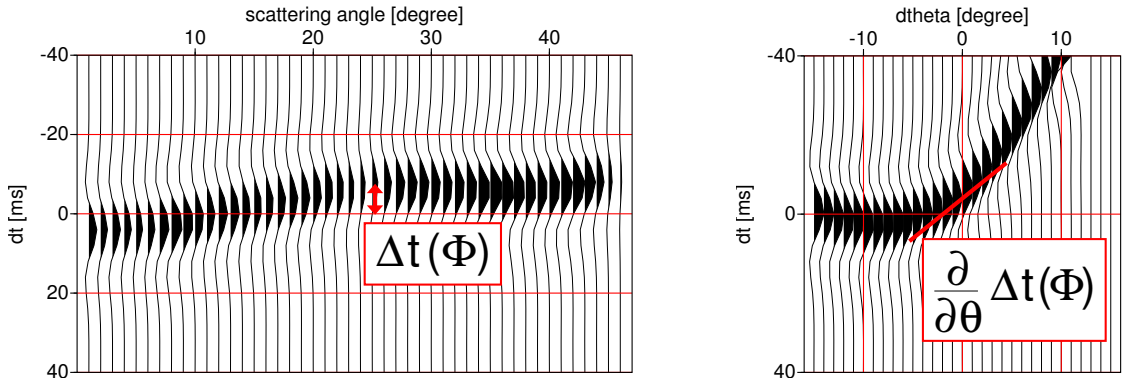

(a) (b)

Figure 7: Time shifted (a) CRP gather and (b) common scattering angle gather in a wrong model. Zero dip in (b) coincides with the estimate of the geological dip.

Computation of Fréchet derivatives

The computation of the first partial derivatives of the traveltime along a ray, the horizontal slowness at the surface, as well as the emergence location of that ray with respect to that ray's initial position and take-off direction as well as with respect to the B-spline coefficients is described for the ZO case in detail in Duveneck (2004). All corresponding derivatives for the finite-offset case are obtained by adding the ones for source and receiver rays. However, instead of horizontal slowness misfits at the surface, time dip residuals $\Delta\,\partial t/\partial\Theta$ are used here. There exists a close relationship between both which makes it possible to use the Fréchet derivatives for horizontal slowness found in Duveneck (2002) and Duveneck (2004).

Picking of time and time dip residuals

Most standard applications parameterize residual moveout by an analytic function, e. g. a parabola, which can then be determined by coherence analysis. However, if the residual moveout deviates from an analytic shape wrong results are obtained. Such a deviation is common in complex models and we observe it in Figure 7(a) which shows a CRP gather taken from the data example presented below. For that reason, I propose a different picking strategy: each trace in the CRP gather is cross-correlated with a part of the ZO trace centered around the picked stationary point. It is assumed that the ZO trace provides a suitable estimate of the wavelet. Picking the maximum in the cross-correlation panel directly gives the time residuals for all scattering angles. This cross-correlation is facilitated by the fact that the CRP gather shows no pulse stretch with increasing scattering angle as it would be observed in a conventional CIG. This is due to the fact that in the time shifting the original sampling of the prestack data is preserved.

Once the traveltime residuals have been determined for all scattering angles the corresponding time dip residuals may be measured by semblance analysis (Neidell and Taner, 1971) along straight lines centered around the a priori geological dip and the picked traveltime misfit in a common-scattering-angle gather (Figure 7(b)).

RELATIONSHIP BETWEEN TIME DIP RESIDUALS IN THE ANGLE DOMAIN AND IN THE MIDPOINT-OFFSET DOMAIN

The diffraction traveltime function $\tau(\Theta,\Phi)$ can be decomposed into source and receiver parts:

$$\tau(\Theta,\Phi) = \tau_S(\Theta,\Phi) + \tau_G(\Theta,\Phi)\ . \tag{11}$$

Using the definition (1) the first partial derivative of τ with respect to the illumination angle Θ reads

$$\frac{\partial \tau}{\partial \Theta} = \frac{\partial \tau_S}{\partial \Theta} + \frac{\partial \tau_G}{\partial \Theta} = \frac{\partial \tau_S}{\partial \gamma_S}\frac{\partial \gamma_S}{\partial \Theta} + \frac{\partial \tau_G}{\partial \gamma_G}\frac{\partial \gamma_G}{\partial \Theta} = \frac{\partial \tau_S}{\partial \gamma_S} + \frac{\partial \tau_G}{\partial \gamma_G} \; . \tag{12}$$

The emergence locations x_S and x_G of shot and receiver ray are functions of the corresponding take-off angle. Therefore, equation (12) may be rewritten in a form relating time dip with respect to illumination angle Θ and horizontal slowness components at source and receiver locations:

$$\frac{\partial \tau}{\partial \Theta} = \frac{\partial \tau_S}{\partial x_S}\frac{\partial x_S}{\partial \gamma_S} + \frac{\partial \tau_G}{\partial x_G}\frac{\partial x_G}{\partial \gamma_G} = \pi_S \frac{\partial x_S}{\partial \gamma_S} + \pi_G \frac{\partial x_G}{\partial \gamma_G} \; , \tag{13}$$

where π_S and π_G denote the horizontal slowness of source and receiver ray building the diffraction traveltime operator. The same derivation can be performed for $\partial\tau/\partial\Phi$ yielding

$$\frac{\partial \tau}{\partial \Phi} = \frac{\partial \tau_S}{\partial x_S}\frac{\partial x_S}{\partial \gamma_S} - \frac{\partial \tau_G}{\partial x_G}\frac{\partial x_G}{\partial \gamma_G} = \pi_S \frac{\partial x_S}{\partial \gamma_S} - \pi_G \frac{\partial x_G}{\partial \gamma_G} \; . \tag{14}$$

Analogous derivatives may be computed for reflection traveltimes. However, these derivatives are taken with respect to non-specular angles as already stated above. Using the horizontal slowness components p_S and p_G the derivatives of reflection traveltime t with respect to illumination angle Θ and scattering angle Φ read

$$\frac{\partial t}{\partial \Theta} = p_S \frac{\partial x_S}{\partial \gamma_S} + p_G \frac{\partial x_G}{\partial \gamma_G} \quad \text{and} \quad \frac{\partial t}{\partial \Phi} = p_S \frac{\partial x_S}{\partial \gamma_S} - p_G \frac{\partial x_G}{\partial \gamma_G} \; . \tag{15}$$

Note the same analogy between angle and midpoint-offset domain already seen in the definition of illumination and scattering angle: the time dip with respect to the illumination angle is the sum of shot and receiver slowness each scaled by a model dependent transformation factor. This is similar to the time dip with respect to the midpoint coordinate which is simply given as sum of shot and receiver slowness. The same analogy is found between time dip with respect to scattering angle and offset. The model dependent factor is the transformation between surface coordinates and ray coordinates defined at the origin of the ray in depth. They are easily computed using dynamic ray-tracing (Červený, 2001).

The difference in time dip with respect to illumination angle Θ between reflection event and diffraction traveltime operator may be written as

$$\begin{aligned} \frac{\partial}{\partial \Theta}\Delta t(\Theta,\Phi) = & \frac{\partial}{\partial \Theta} t(\Theta,\Phi) - \frac{\partial}{\partial \Theta}\tau(\Theta,\Phi) = \\ & (p_S - \pi_S)\frac{\partial x_S}{\partial \gamma_S} + (p_G - \pi_G)\frac{\partial x_G}{\partial \gamma_G} = \Delta p_S \frac{\partial x_S}{\partial \gamma_S} + \Delta p_G \frac{\partial x_G}{\partial \gamma_G} \; . \end{aligned} \tag{16}$$

A similar expression is derived in the same way for the time dip difference with respect to scattering angle Φ:

$$\begin{aligned} \frac{\partial}{\partial \Phi}\Delta t(\Theta,\Phi) = & \frac{\partial}{\partial \Phi} t(\Theta,\Phi) - \frac{\partial}{\partial \Phi}\tau(\Theta,\Phi) = \\ & (p_S - \pi_S)\frac{\partial x_S}{\partial \gamma_S} - (p_G - \pi_G)\frac{\partial x_G}{\partial \gamma_G} = \Delta p_S \frac{\partial x_S}{\partial \gamma_S} - \Delta p_G \frac{\partial x_G}{\partial \gamma_G} \; . \end{aligned} \tag{17}$$

To obtain these time dip differences along the CRP trajectory, all derivatives in equation (16) and equation (17) have to be taken at the geological dip $\Theta = \Theta_0$.

DATA EXAMPLE

The first data example is as sparse as possible. It makes use of only one pick in a ZO section. I will not show the inverted velocity model because it can not be assumed that a reasonable model is obtained under such circumstances. However, this example clearly demonstrates the meaning of fitting a CIG and a CRP gather kinematically.

Starting from the same initial model, three different inversions have been performed, each with two iterations. For the first one I used only ZO data and traveltime residuals picked in a CIG. For the second

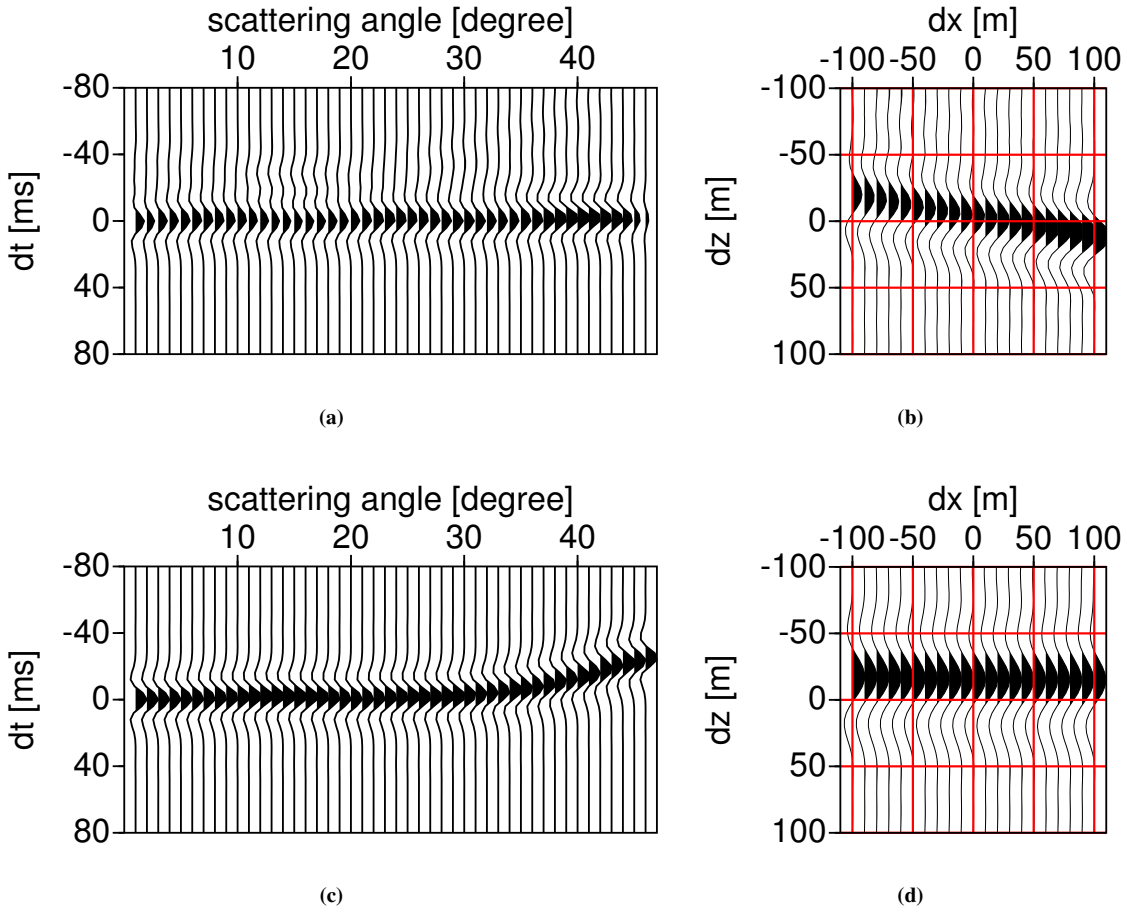

Figure 8: Inversion results using traveltime residuals picked in a CIG, no dip residuals included in the inversion: (a) flat CIG, (b) depth migrated reflector segment for offset 0 m, (c) CRP gather, (d) depth migrated reflector segment for offset 3800 m

one I used only ZO data and traveltime residuals picked in a CRP gather. No time dip residuals have been used in these inversions. In the third one the inversion scheme presented above has been applied. The inversion results are summarized in Figures 8, 9, and 10, respectively. Each figure shows the CRP gather and the CIG associated with the ZO pick. The CIG has been obtained applying the necessary half time derivative to the time shifted prestack data cube and summing over the illumination angle. Additionally, depth migrated common offset sections are shown. They are centered around the depth position obtained in the corresponding inversion. Note that this position is different in all three inversion results.

After the first inversion the CIG is flat. However, the CRP gather is non-flat. Thus, CIG and CRP gather are not kinematically equivalent. This results in different dips of the reflector segment associated with the ZO pick in common offset depth migrated sections.

After the second inversion the CRP gather is flat whereas the CIG shows significant residual moveout. This results not only in different dips for different offsets of the reflector segment associated with the ZO pick, but also the depth location after migration differs from offset to offset.

Applying the inversion scheme as presented in this paper a result is obtained where the CIG and the CRP gather are kinematically equivalent, both are flat. This is due to the use of time dip residuals in the inversion. Minimization of the time dip residuals leads to a consistent geological dip of the reflector segment. Although the obtained velocity model, depth position, and geological dip are not the true values, a model has been obtained which is kinematically consistent with the prestack data. This, of course, holds

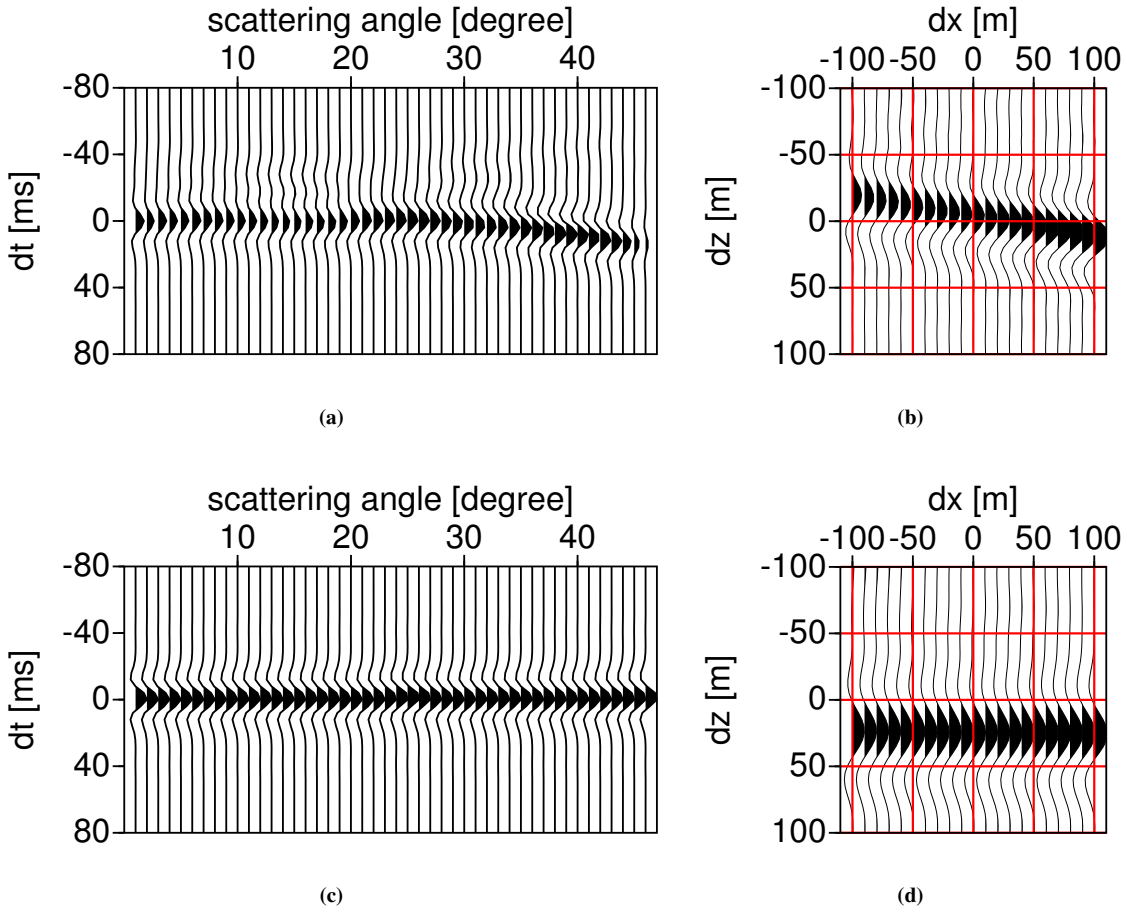

Figure 9: Inversion results using traveltime residuals picked in a CRP gather, no dip residuals included in the inversion: (a) CIG, (b) depth migrated reflector segment for offset 0 m, (c) flat CRP gather, (d) depth migrated reflector segment for offset 3800 m

only for the selected ZO location.

The second data example uses a complete synthetic prestack data set with offsets up to 4000 m. For this data a ZO section has been obtained by application of the common-reflection-surface (CRS) stack technique (see, e. g., Jäger, 1999). In this section, 412 pick locations have been selected automatically using the technique presented in Klüver and Mann (2005). The CRS stacked section together with the pick locations is shown in Figure 11. For each pick location the quantities characterizing the ZO stationary point have been extracted and calculated from the CRS attribute sections. The velocity model has been described by 29 nodes in horizontal direction with a spacing of 400 m and 18 nodes in vertical direction with a spacing of 200 m. The velocity at the surface has been set to the true value of 2000 m/s and a constant vertical gradient of $0.67\,\mathrm{s}^{-1}$ has been applied initially. All pick locations have been mapped to depth by normal ray tracing to obtain the corresponding initial estimates of depth position and geological dip. Then, six iterations of the presented inversion scheme have been performed. In all iterations the depth locations and geological dips obtained in the previous iteration have been used; no recalculation of these quantities by normal ray tracing has been applied. Figure 12 shows the obtained depth positions on top of the true, blocky velocity model used for modeling the prestack data. The obtained depth positions fit the reflector structure quite well. The same holds for the prestack depth migration result. It has been overlaid on the true velocity model in Figure 14. Figure 13 shows the smooth velocity model obtained by the inversion. On top, the prestack migration result is displayed again. The smooth velocity distribution fits the reflector structure

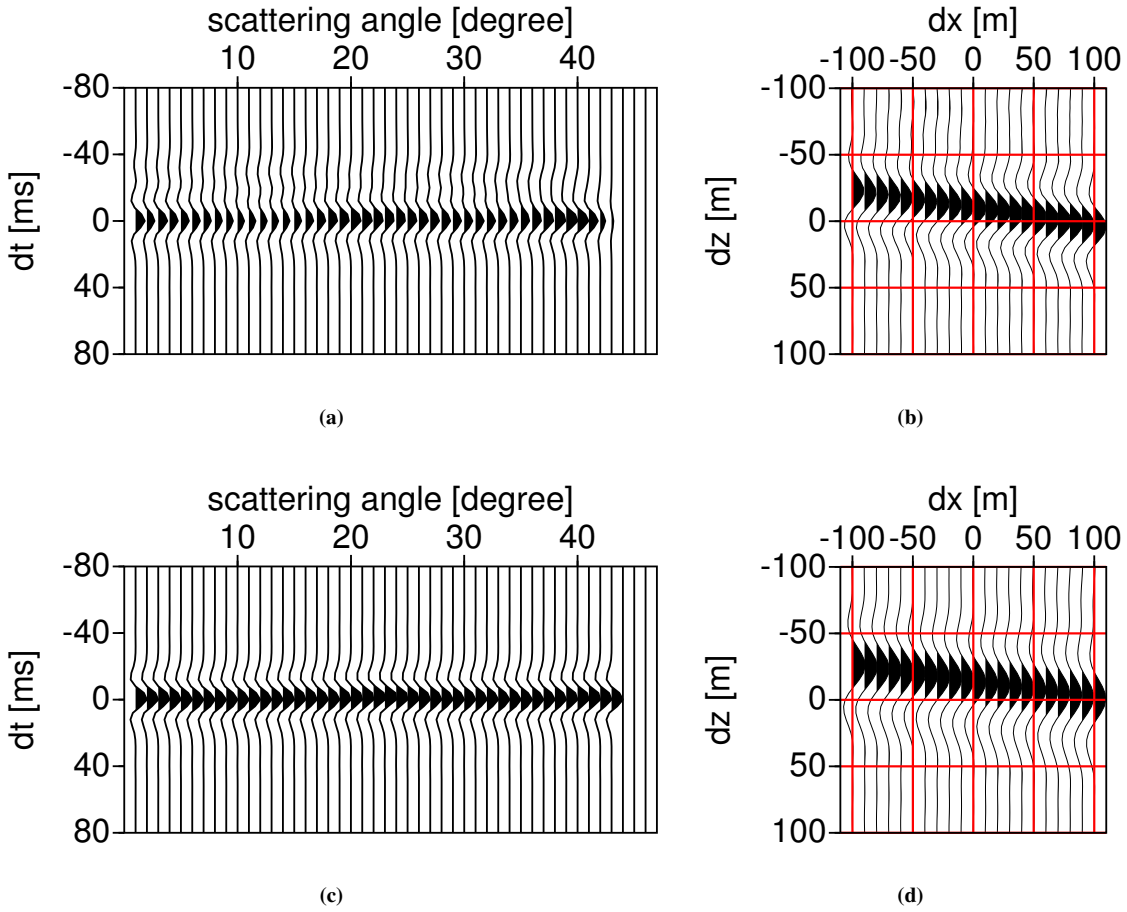

Figure 10: (a) flat CIG, (b) depth migrated reflector segment for offset $0\,m$, (c) flat CRP gather, (d) depth migrated reflector segment for offset $3800\,m$

quite well. Generally, a large degree of similarity can be observed comparing the true velocity model and the inversion result. Figure 15 shows selected CIGs obtained by conventional Kirchhoff prestack depth migration. They are all reasonably flat. All these results demonstrate the success of the presented method.

CONCLUSIONS

In this paper, I have presented a new inversion scheme which provides smooth depth velocity models leading to accurate migration results. The method uses isolated picks identified in a poststack ZO section. Each pick represents an estimate of a ZO stationary point. Using the associated diffraction traveltime operators as moveout function, time and time dip residuals are determined. These residuals represent quantities defined in the post-migrated domain. However, the presented technique allows to extract them without performing a complete prestack depth migration. Time and time dip residuals are picked in a non-parametric way. Therefore, the method has no intrinsic limitation regarding the complexity of residual moveout. Equations have been derived which relate the time dip difference with respect to the illumination angle between the forward-modeled diffraction traveltime operator and the reflection event in the prestack data to slowness misfits at the source and receiver locations. A first test on a synthetic data example clearly demonstrates the potential of the presented method.

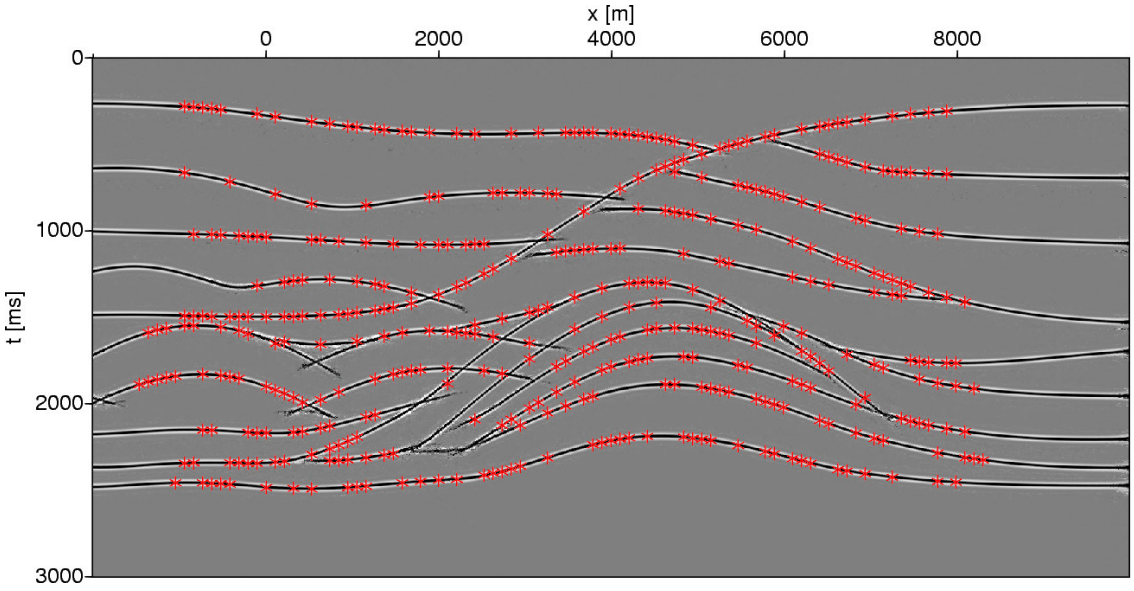

Figure 11: ZO section with 412 selected pick locations.

ACKNOWLEDGMENTS

This work was kindly supported by the sponsors of the *Wave Inversion Technology (WIT) Consortium*, Karlsruhe, Germany.

REFERENCES

Červený, V. (2001). *Seismic ray theory*. Cambridge University Press, Cambridge.

de Boor, C. (1978). *A practical guide to splines*. Springer-Verlag, Berlin.

Duveneck, E. (2002). Tomographic velocity model inversion with CRS attributes. In *Ann. Report*, volume 6, pages 92–106. Wave Inversion Technology Consortium.

Duveneck, E. (2004). *Tomographic determination of seismic velocity models with kinematic wavefield attributes*. Logos Verlag, Berlin.

Jäger, R. (1999). The Common Reflection Surface stack – theory and application. Master's thesis, University of Karlsruhe.

Klüver, T. and Mann, J. (2005). Event-consistent smoothing and automated picking in CRS-based seismic imaging. In *Expanded abstracts, 75rd Ann. Internat. Mtg.* Soc. Expl. Geophys.

Menke, W. (1984). *Geophysical data analysis: discrete inverse theory*. Academic Press, Orlando.

Neidell, N. S. and Taner, M. T. (1971). Semblance and other coherency measures for multichannel data. *Geophysics*, 36(3):482–497.

Paige, C. C. and Saunders, M. A. (1982a). Algorithm 583 – LSQR: sparse linear equations and least squares problems. *ACM Trans. Math. Softw.*, 8(2):195–209.

Paige, C. C. and Saunders, M. A. (1982b). LSQR: an algorithm for sparse linear equations and sparse least squares. *ACM Trans. Math. Softw.*, 8(1):43–71.

Stork, C. (1992). Reflection tomography in the postmigrated domain. *Geophysics*, 57(5):680–692.

Tarantola, A. (1987). *Inverse problem theory: methods for data fitting and model parameter estimation*. Elsevier, Amsterdam.

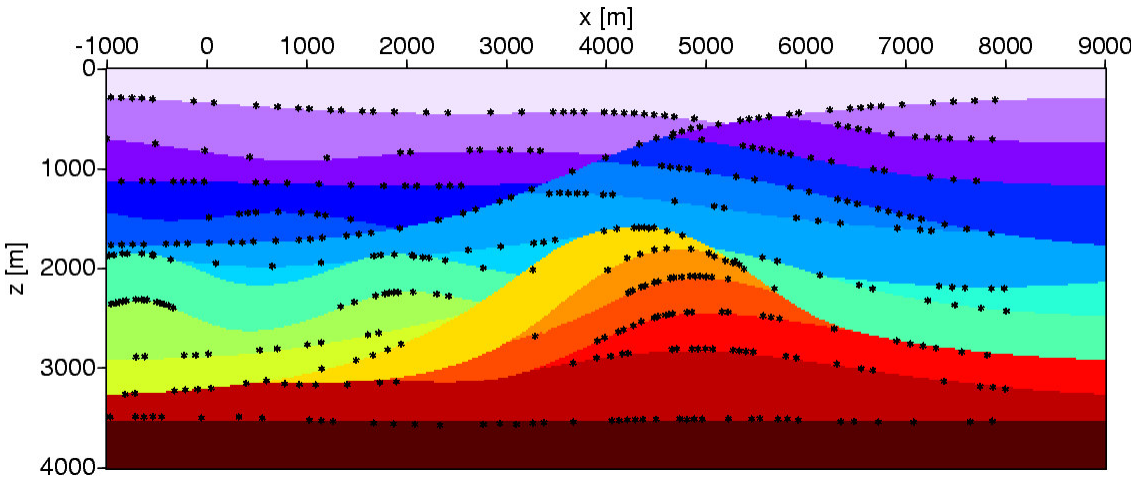

Figure 12: Inverted depth locations plotted into the true, blocky velocity model.

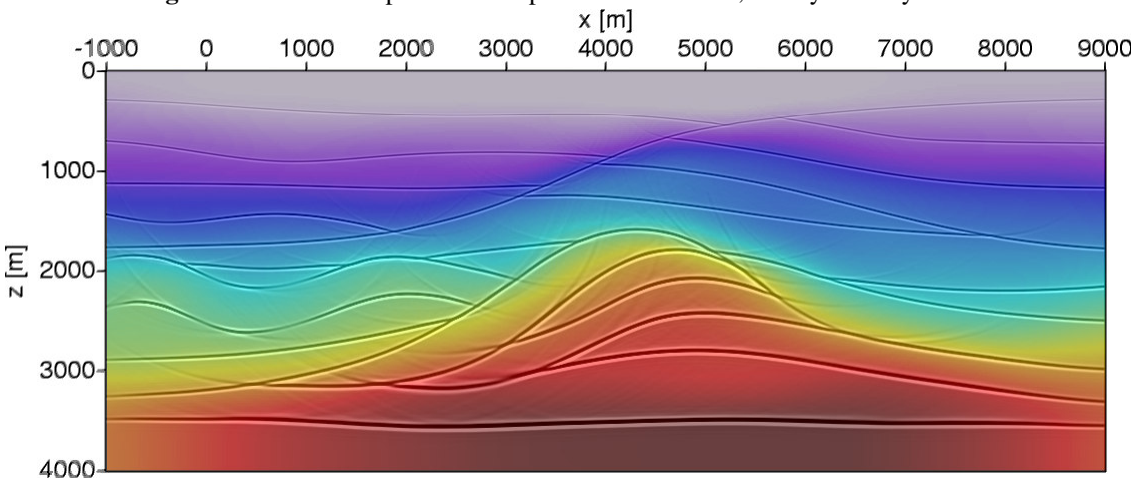

Figure 13: Inverted smooth velocity model overlaid with prestack depth migration result.

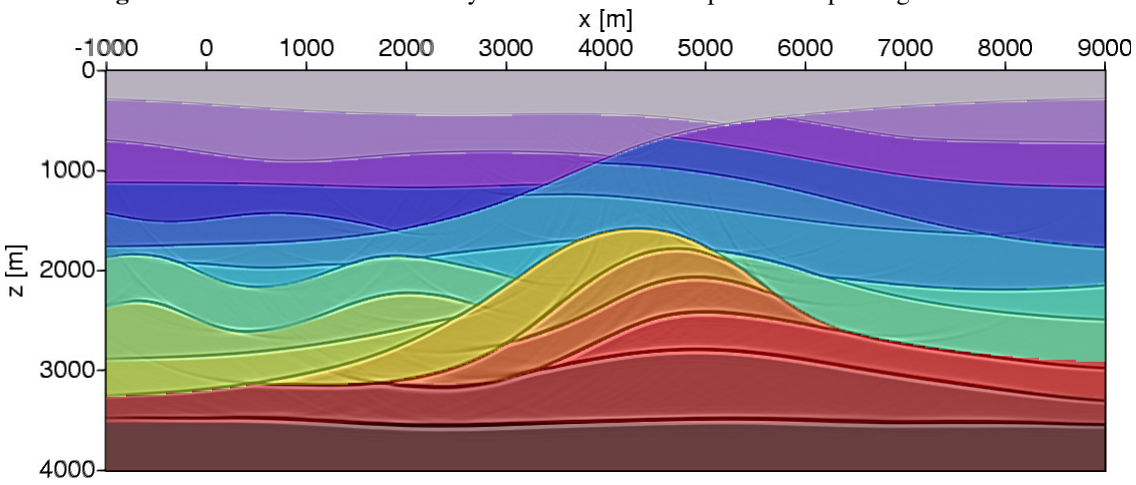

Figure 14: Prestack depth migrated section using inverted velocity model on top of the true, blocky velocity model.

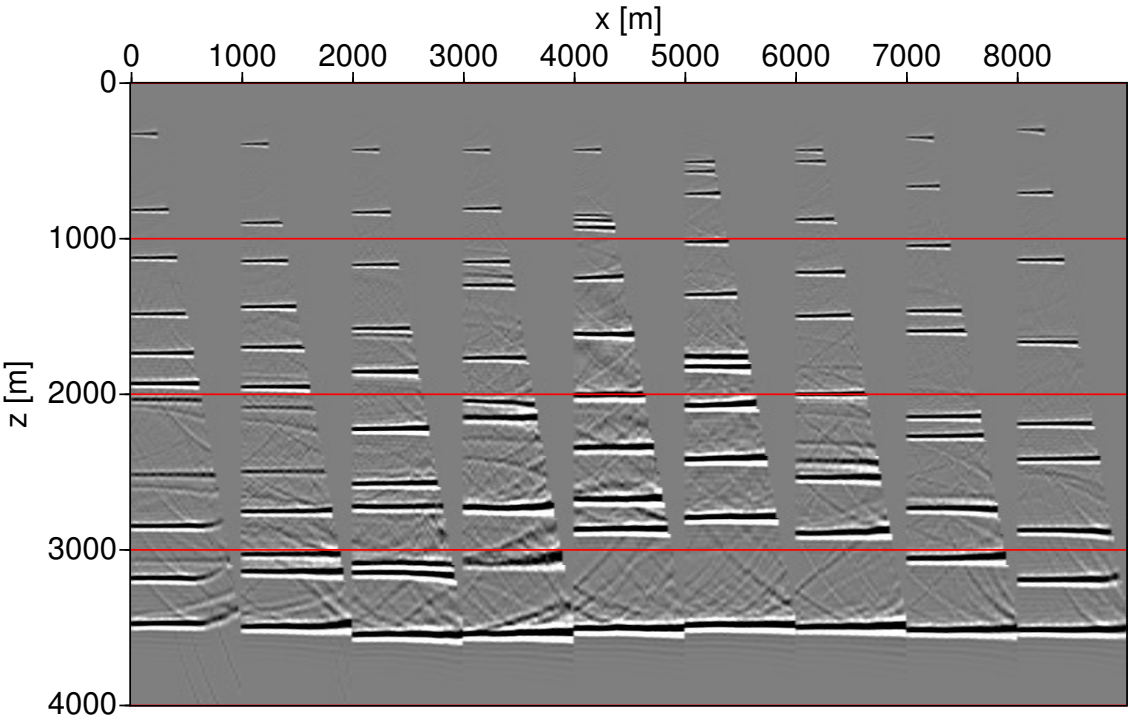

Figure 15: Selected CIGs.